

Scientific paper

In Situ and *Ex Situ* TEOS Coating of ZnO Nanoparticles and the Preparation of Composite ZnO/PMMA for UV-VIS Absorbers

Dajana Japić,¹ Igor Djerdj,² Marjan Marinšek³ and Zorica Crnjak Orel^{1,4,*}¹ National Institute of Chemistry Slovenia, Hajdrihova 19, 1001 Ljubljana, Slovenia² Ruđer Bošković Institute, Bijenička 54, 10000 Zagreb, Croatia³ Faculty of Chemistry and Chemical Technology, University of Ljubljana, Aškerčeva cesta 5, 1000 Ljubljana Slovenia⁴ Centre of excellence Polimat, Tehnološki park 24, 1000 Ljubljana, Slovenia

* Corresponding author: E-mail: zorica.crnjak.orel@ki.si

Received: 10-06-2013

Abstract

ZnO nanoparticles were prepared in a typical single-step experimental procedure, in different water-to-ethylene glycol volume ratios at a moderate temperature. Morphological studies performed by SEM and TEM have revealed two different types of nanosized particles: hexagonal faceted nanoparticles and spherical ones. The obtained ZnO nanoparticles were further coated with the coupling reagent tetraethyl orthosilicate (TEOS), *in situ* and *ex situ*. The thickness of the silica layer around the ZnO nanoparticles varied between 4 and 18 nm. The coated as well as the bare ZnO nanoparticles were thoroughly characterized by different characterization methods. They were also incorporated into poly-methylmethacrylate (PMMA). The obtained PMMA/ZnO nanocomposites showed relatively high transmittance for visible light but also relatively high absorbance in the UV region between 250–370 nm.

Keywords: Silica coated ZnO nanoparticles; tetraethyl orthosilicate, PMMA/ZnO composite;

1. Introduction

Zinc oxide is inorganic multifunctional material with many useful properties. It is used in a wide range of applications, including the catalysts, colour hue, in cosmetics as a UV absorber, in biomedical applications, thin films, chemical sensors, electroluminescent devices, etc.^{1–9} Zinc oxide nanoparticles can be synthesized in several different ways: homogeneous precipitation,¹⁰ spray pyrolysis,¹¹ the sol-gel method,^{12–14} the chemical method¹⁵ (hydrothermal¹⁶ and solvothermal^{17–19}).

The development of coated structured²⁰ nano-materials has recently been attracting extensive attention. In general, the coating of particles is used to improve their stability and dispersability in suspensions. In addition, coated particles can be used for various applications in nanofabrication, nanopatterning, self assembly, biopro-

bes, drug delivery, pigments, photocatalysis, as substrates for functional coatings, printing, UV inks, e-print, optical communications (security papers), protection, barriers, portable energy sensors, photocatalytic wallpaper with antibacterial activity, etc.^{21–23} Another reason for coating nanoparticles is to reduce the potential for photocatalysis, and the formation of free radicals and reactive oxygen species, in particular for sunscreen applications.²¹ For coatings of nanoparticles, silica was the most studied shell candidate; it has good environmental stability and compatibility with many different materials.^{20,24–26} For instance, Selegård et al. prepared coated ZnO particles with (3-mercaptopropyl)trimethoxysilane with a high potential for recognition studies in biosensing applications.²⁷ ZnO nanoparticles were further coated with 3-methacryloxypropyltrimethoxysilane (KH570)²⁸. Wu, et al.⁵ presented six different types of coating reagents for coating ZnO nanocrystals: 3-aminopropyl trimethoxysi-

lane (Am), 3-aminopropyl triethoxysilane (APTES)^{29,30} tetraethyl orthosilicate (TEOS),^{31–33} mercaptosuccinic acid (Ms), 3-mercaptopropyl trimethoxysilane (Mp) and polyvinylpyrrolidone (PvP). In their study, they performed the synthesis of ZnO nanoparticles at rather moderate temperature (68 °C) using bio-compatible coating agents. The described coating reagents had a triple function: to control the particle size of ZnO, to provide a side group on the surface of ZnO, and to eliminate the surface defect of the ZnO nanocrystals. It was found that the first three coating reagents limited the growth of ZnO nanoparticles, while the last two caused even larger ZnO clusters in the suspension. ZnO nanoparticles can be also coated with different organic acids, such as benzoic-, nicotinic-, and cinnamic-acid or nonaromatic formic-acid.³⁴ In recent decades, the preparation of inorganic particles incorporated in nanocomposites³⁵ with polymers has become very important. Such nanocomposites have attractive optical,³⁶ thermal, mechanical, magnetic and electric properties^{29,37,38} These nanocomposites have potential application in electronics,³⁹ rubber reinforcement⁴⁰ coatings,^{41,42} etc. There are several different types of nanocomposites prepared from various inorganic particles with numerous polymer materials, such as poly(methylmethacrylate) PMMA,⁴³ styrene,⁴⁰ polypropylene,⁴⁴ etc. PMMA is used as a substitute for inorganic glass, due to higher impact strength and favourable processing conditions.⁴⁵ Nanocomposites of ZnO/PMMA have potential applications for UV protecting sheets^{46,47} and films,⁴⁸ and materials with high improved thermal stability.^{49–51}

In this study, the coating of ZnO nanoparticles with silica (TEOS) is described. The main goal was to prepare coated hexagonal and spherical ZnO nanoparticles. In addition, the paper is focused on two different ways of ZnO nanoparticles' coating (*in situ* and *ex situ*). We studied the influence of various additives on the thickness of silica layer around the ZnO particles and their incorporation into PMMA.

2. Experimental

2.1. Materials and Methods

All reagents used for synthesis were of an analytical reagent grade. To avoid hydrolysis upon storage, fresh stock aqueous solutions were prepared from Zn(NO₃)₂ · 6H₂O (98% Merck), ethylene glycol (99.5% Sigma-Aldrich), lithium hydroxide (98% Sigma-Aldrich). For *in situ* and *ex situ* coating of ZnO particles, tetraethyl orthosilicate (TEOS) (Sigma-Aldrich), 25% NH_{3(aq)} solution (Merck) and absolute EtOH (Sigma-Aldrich) were used. Methyl methacrylate (MMA) (99% Sigma-Aldrich), bis (4-t-butylcyclohexyl)-peroxydicarbonate (P-16) and dilauroyl peroxide (LPO) were used for the preparation of ZnO/PMMA nanocomposites.

2.2. Synthesis of Hexagonal and Spherical ZnO Nanoparticles

The selected concentrations of Zn²⁺ ions (prepared from Zn(NO₃)₂ · 6H₂O and LiOH) in the experiments were 0.1 M. Two different volume ratios of water-to-ethylene glycol ($V(\text{H}_2\text{O}):V(\text{EG}) = 1:5$ and $V(\text{H}_2\text{O}):V(\text{EG}) = 5:1$) were employed. The syntheses of ZnO nanoparticles were carried out in a 250 mL flask without stirring at 100 °C, for 2 hours. Firstly, Zn²⁺ and LiOH solutions in 150 mL of mixed solvents were prepared and heated to 100 °C. After the hydrolysis reaction was completed, the resulting white precipitate of ZnO was centrifuged, washed with water four times and dried in air at room temperature or re-dispersed in EtOH.

2.3. The Preparation of Silica Coated ZnO Nanoparticles by Ex Situ and in Situ Method

The synthesized ZnO nanoparticles were further functionalized by coating them with silica. In the first case (the *ex situ* method), ZnO nanoparticles were first prepared and then kept in mother solution or re-dispersed in EtOH. The four concentrations of TEOS used for coating of ZnO particles were 0.048 M, 0.024 M, 0.001 M and 0.0003 M. In a typical *ex situ* coating process, the dried ZnO was re-dispersed in 10 mL EtOH and 4 mL MQ water, then NH_{3(aq)} was added to the re-dispersed ZnO solution, and finally the appropriate quantity of TEOS was admixed (Table 1). The coating process was carried out at room temperature for 1 hour in an ultrasonic bath, as suggested in the literature.³¹ After the procedure was completed, the final product was purified in EtOH and dried in air at room temperature.

In a typical *in situ* method, the preparation of ZnO nanoparticles was basically the same, except that TEOS was added to the initial reaction mixture prior to the synthesis of ZnO nanoparticles.

2.4. Preparation of ZnO/PMMA Nanocomposites

Bare or coated ZnO powders were suspended in 5 mL of MMA in a centrifuge tube (0.1% ZnO, 0.15% the *in situ* coated ZnO or 0.2% the *ex situ* coated ZnO). The suspensions were sonicated for 20 minutes prior to the addition of initiators bis (4-t-butylcyclohexyl)-peroxydicarbonate (P-16) (0.25 wt.%) and dilauroyl peroxide (LPO) (0.25 wt.%). The polymerization of MMA was carried out in water bath at 60 °C for 1 hour. PMMA with dispersed ZnO nanoparticles was poured into glass plates and placed in an oven for 2 hours at 55 °C and subsequently for 10 minutes at 120 °C. Finally, the PMMA/ZnO sheets were separated from the glass plate moulds. The additions of solid particles were optimized with respect to the absorption of light in the UV region.

2. 5. Caffeine Photocatalytic Degradation

Degradation of caffeine (as a model substance for the photocatalytic activity of ZnO particles) over time was set as follows. The coated or non-coated ZnO particles (40 mg) were admixed to a caffeine ($C_8H_{10}N_4O_2$) aqueous solution (50 mL, 10^{-4} M). The obtained suspension was then stirred for 20 minutes. The mixture was placed into a chamber (Kambič, type I-265 CKUV) equipped with UV lamp for the measurement of photocatalytic degradation. Samples were collected at regular time intervals and centrifuged to remove solid particles prior to the caffeine concentration analysis. The UV-VIS absorption of the solution was measured from 225 nm to 350 nm from which the caffeine-relative concentration was calculated.

2. 6. Products Characterization

Products were characterized with IR spectroscopy (FTIR spectrometer, Perkin Elmer 2000) in the spectral range between 4000 and 360 cm^{-1} with a spectral resolution of 4 cm^{-1} in the transmittance mode. The KBr pellets with 1 wt % of sample were used for the IR analysis. Field emission scanning electron microscopy (FE-SEM, Zeiss Supra 35 VP equipped with EDS detector and the ability to work in STEM mode), and X-ray powder diffraction (XRD, Siemens D-500 X-ray diffractometer) were used for the careful morphological and structural characterization. TEM observations were carried out in a transmission electron microscope operated at 200 kV (JEM-2100, JEOL) which was equipped with EDX. TEM samples were prepared by dispersing the powders in ethanol, using an ultrasonification followed by the deposition of the obtained suspension on carbon-coated copper grids. The zeta potential of ZnO and coated ZnO powder suspensions was measured using the 501 Lazer Zee MeterTM, PenKem Inc. The pH adjustments during the zeta potential measurements were achieved by adding dilute aqueous NaOH (0.1 M) or concentrate HCl (11.9 M) solutions. The UV-VIS spectra of ZnO/PMMA nanocomposites were measured using the Perkin Elmer Lambda 950 UV-VIS spectrometer in the spectral range between 250 and 800 nm. TG investigations of ZnO/PMMA nanocomposites were carried out at a constant flow of Ar-O₂ (18 L/h) in the temperatu-

re range between (30–600 °C) using the Mettler TA4000 instrument. For the kinetic analysis, TG experiments were repeated under non-isothermal conditions at heating rates β from 2 K/min to 10 K/min. Measurements of the dynamic light scattering (DLS) analysis were performed on a ZetaSizer Nano ZS instrument.

3. Results and Discussion

ZnO nanoparticles were prepared by the addition of $Zn(NO_3)_2 \cdot 6H_2O$ and LiOH (0.1 M) in various water-to-ethylene glycol volume ratios as described in the experimental work and summarized in Table 1. ZnO particles were coated by two different methods (*in situ* and *ex situ*). In the present work, we varied the concentration of coating reagent and studied its impact on thickness of the coating layer. The experimental parameters of eight selected samples are presented in Table 1.

The SEM micrographs of coated ZnO products prepared by the *ex situ* method are presented in Figs 1–2. Samples were prepared by admixing dry ZnO nanoparticles into EtOH and water and coated with the lowest concentration of TEOS. The micrograph presented in Figure 1 shows faceted crystals of coated hexagonal shaped ZnO with diameters around 100 nm (sample 1). In Figure 2, the micrograph shows spherical ZnO nanoparticles (dia-

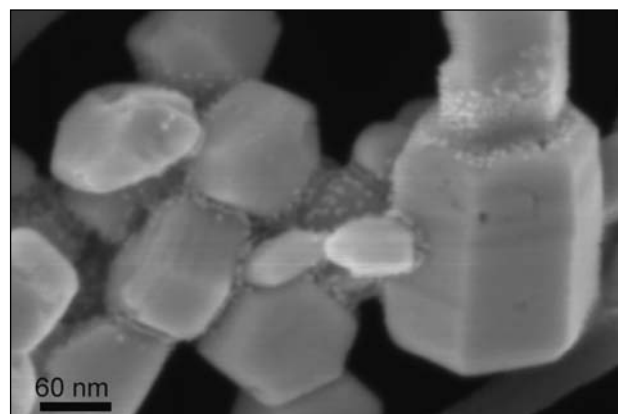


Figure 1: SEM micrograph of silica-coated hexagonal ZnO nanoparticles (sample 1) prepared with the *ex situ* method.

Table 1 The parameters for ZnO coating by the *ex situ* or the *in situ* methods.

Sample	$V_{H_2O}:V_{EG}$	coating method	shape of ZnO particles	m_{ZnO} used for coating (mg)	c (M) (TEOS)
1	5:1	<i>Ex situ</i>	hexagonal	22.0	0.0003
2	1:5	<i>Ex situ</i>	spherical	22.0	0.0003
3	5:1	<i>Ex situ</i>	hexagonal	226.4	0.0240
4	1:5	<i>Ex situ</i>	spherical	202.8	0.0240
5	5:1	<i>Ex situ</i>	hexagonal	226.4	0.0480
6	1:5	<i>Ex situ</i>	spherical	202.8	0.0480
7	5:1	<i>In situ</i>	undefined	/	0.0010
8	1:5	<i>In situ</i>	undefined	/	0.0010

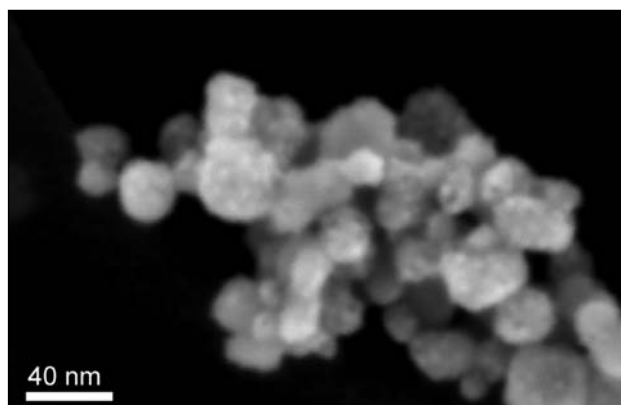


Figure 2: SEM micrograph of silica coated spherical ZnO nanoparticles (sample 2) prepared with the *ex situ* method.

meter ≈ 50 nm) coated with a layer of silica (sample 2). For samples 1 and 2, we observed that the silica coating had no influence on the morphology of the ZnO nanoparticles.

When a higher concentration of TEOS was added (samples 3 and 4 ($c(\text{TEOS}) = 0.0240$ M)), SEM images (not shown) revealed an increase in nanoparticles agglomeration. The higher degree of agglomeration after the ZnO coating was observed mostly for spherical nanoparticles (sample 4), which can be ascribed to their smaller size: smaller nanoparticles tend to agglomerate more intensely. Similar behaviour was observed for sample 3.

The micrographs of samples 7 and 8 are presented in Figures 3 and 4, respectively. Both samples were prepared with the *in situ* coating method with TEOS. The experimental conditions of samples 7 and 8, regarding the initial concentrations of Zn^{2+} , LiOH and solvents mixture, should lead to the formation of hexagonal and spherical ZnO nanoparticles, respectively. However, we observed that in both samples silica affected the morphology of the ZnO nanoparticles, which became more irregularly shaped.

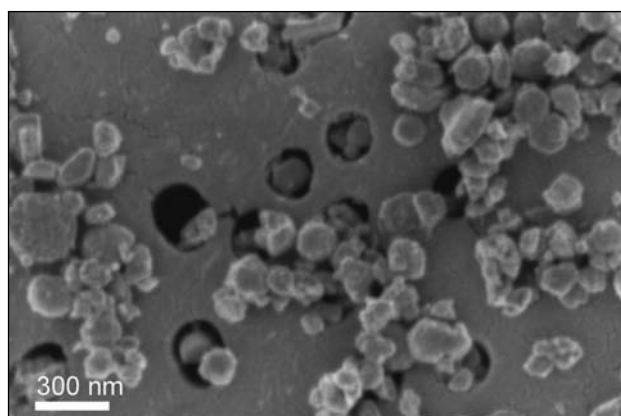


Figure 3: FE-SEM micrograph of sample 7 prepared with the *in situ* method.

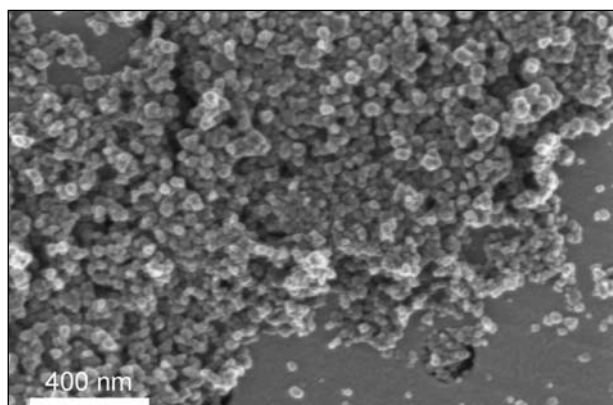


Figure 4: FE-SEM micrograph of sample 8 prepared with the *in situ* method.

TEM images of dried, re-dispersed and coated ZnO nanoparticles are shown in Figure 5 – Figure 12. The TEM image of sample 1 (Figure 5) revealed the hexagonal ZnO nanoparticles with a silica layer of thickness ≈ 5 nm. The measured thickness of the silica layer for sample 2 was ≈ 4 nm (Figure 6).

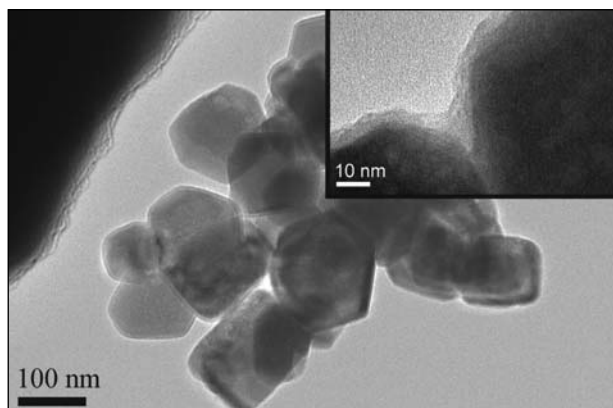


Figure 5: TEM/HRTEM image of coated hexagonal ZnO nanoparticles (sample 1).

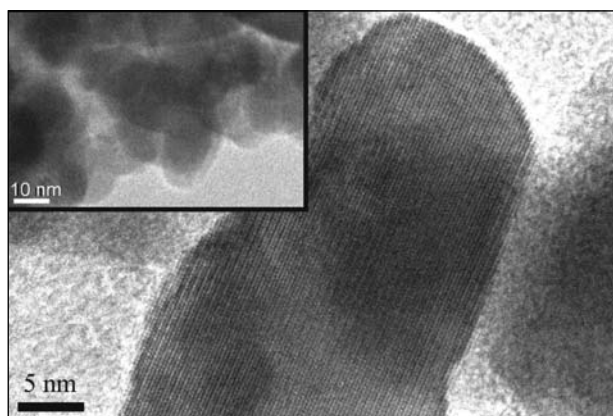


Figure 6: TEM/HRTEM images of coated spherical ZnO nanoparticles (sample 2).

Samples 3 and 4 ($c(\text{TEOS}) = 0.0240 \text{ M}$) were coated in mother solutions of ZnO and not by re-dispersing the dried ZnO in EtOH. In both cases, higher amounts of added silica were also used. The main difference when comparing samples 1 and 2 with samples 3 and 4 was in the thickness of the shell silica layer. The silica layer thickness in sample 3 was $\approx 7 \text{ nm}$ and is clearly visible in Figure 7, while coated spherical nanoparticles in sample 4 exhibited silica layers with a thickness of $\approx 11 \text{ nm}$ (Figure 8).

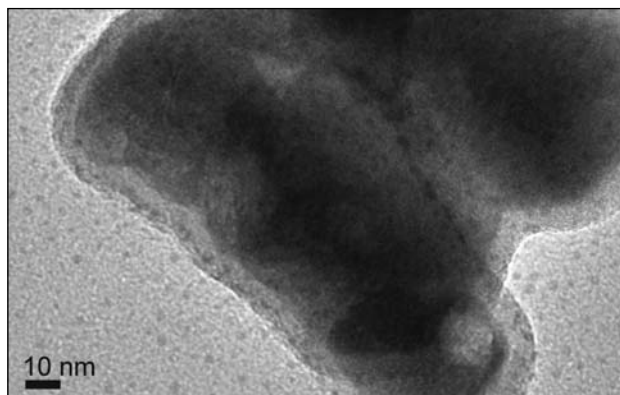


Figure 7: TEM image of ZnO nanoparticles (sample 3).

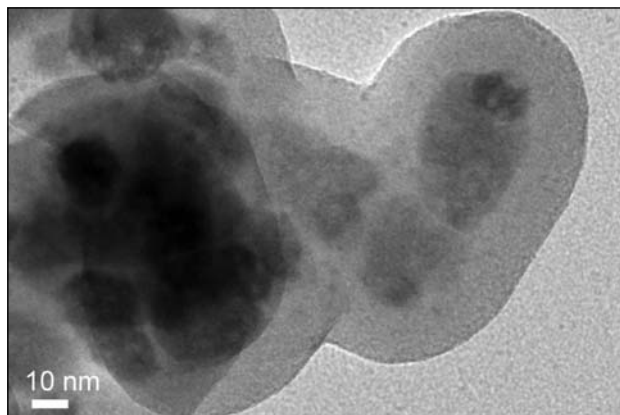


Figure 8: TEM image of the coated spherical ZnO nanoparticles (sample 4).

The amount of added TEOS was further increased during the preparation of samples 5 and 6 ($c(\text{TEOS}) = 0.0480 \text{ M}$). However, the thickness of the silica layer around the hexagonal ZnO particles (Figure 9) was not significantly increased ($\approx 8 \text{ nm}$). However, the thickness of silica layer was clearly increased ($\approx 18 \text{ nm}$) in the case of spherical ZnO nanoparticles, which is presented in Figure 10.

The TEM images (Figure 11 and Figure 12) show coated ZnO nanoparticles (samples 7 and 8) prepared with the *in situ* coating method. In both cases, the added amount of TEOS reagent was ($c(\text{TEOS}) = 0.0010 \text{ M}$). In contrast to the *ex situ* coating process, where the silica la-

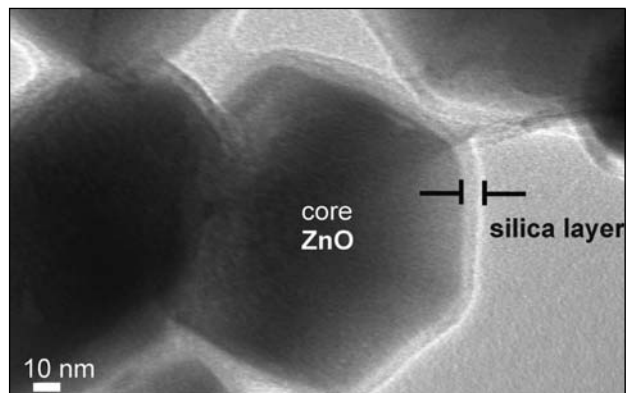


Figure 9: TEM image of coated hexagonal ZnO nanoparticles (sample 5).

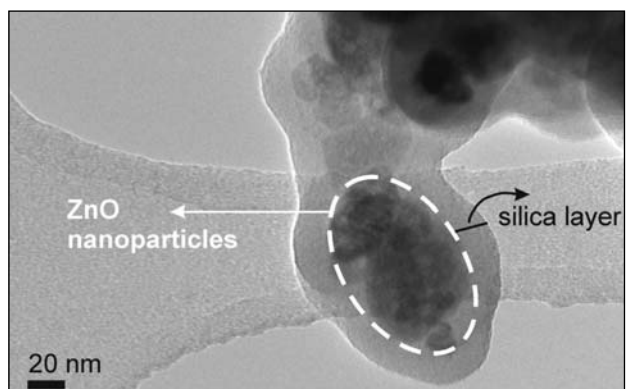


Figure 10: TEM image of coated spherical ZnO nanoparticles (sample 6).

yer did not change the shape of ZnO nanoparticles, the *in situ* coating process clearly influenced the formed particles morphology. Instead of well-defined particles, experiments 7 and 8 yielded nanoparticles of an undefined shape. Furthermore, the *in situ* coating process did not produce clear shell-core particle structures. Instead, the outer layer of the prepared particles was probably zinc silicate. This fact implies that TEOS was deposited on each new layer of the growing particle changing not only its morphology but also chemical composition and structure.

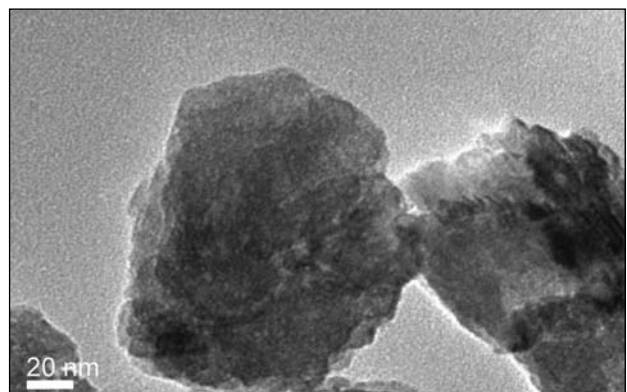


Figure 11: TEM image of nanoparticles (sample 7).

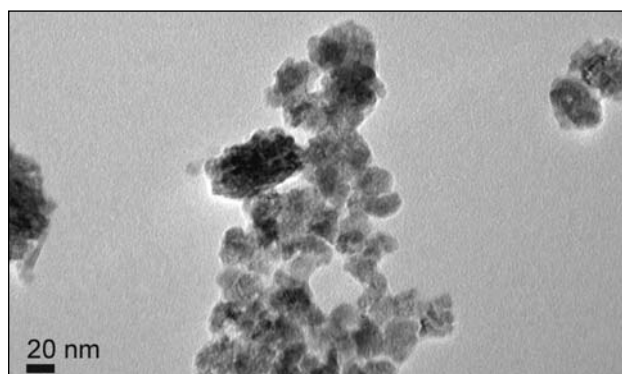


Figure 12: TEM image of nanoparticles (sample 8).

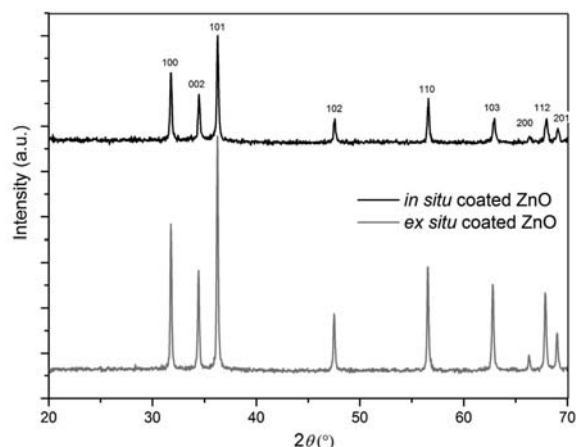


Figure 13: XRD diffractogram of coated samples prepared by two different coating methods.

Powder XRD patterns of samples prepared via different coating methods are presented in Figure 13. The major peaks in Figure 13 correspond to ZnO zincite (JCPDS 01-079-2205, zinc oxide).

The FTIR spectra of samples prepared by the *ex situ* method are presented in Figure 14a. The IR spectra confirmed the formation of ZnO due to presence of stretching mode bands in the range from 600 up to 370 cm^{-1} . The presence of NO_3^- group (1384 cm^{-1}) was confirmed in all products prepared by the *ex situ* method. The IR band at 797 cm^{-1} and the broad IR band in the range between 980 and 1200 cm^{-1} was ascribed to the characteristic Si–O–Si asymmetric stretching vibration.⁵² We can suppose that SiO_2 shells were created by the hydrolysis and condensation of TEOS.²⁰

The FTIR spectra of samples prepared by the *in situ* method are presented in Figure 14b. Again we can confirm the formation of ZnO due to presence of stretching mode bands in the range from 600 up to 370 cm^{-1} . Nitrate bonds (IR band at 1384 cm^{-1}) were also present in both products prepared by the *in situ* method. In contrast to the samples prepared by the *ex situ* method, we observed some vibrations in the range between 900–1000 cm^{-1} .^{53,54} This broad IR band indicates the presence of amorphous

zinc silicate Zn_2SiO_4 .⁵⁵ Since zinc silicate cannot be confirmed by the XRD analysis, its layers clearly grow as an amorphous phase.

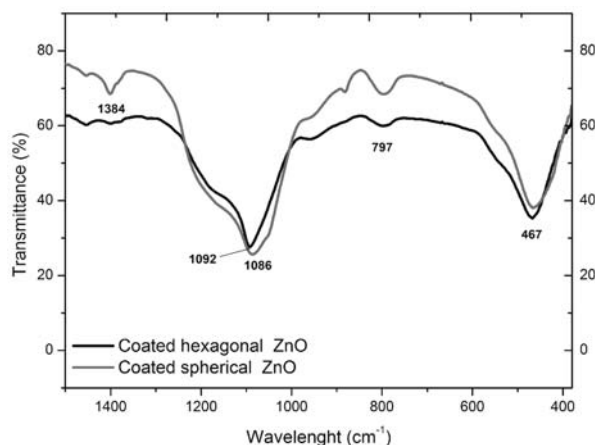


Figure 14a: FTIR spectra of samples prepared with the *ex situ* method for spherical and hexagonal nanoparticles.

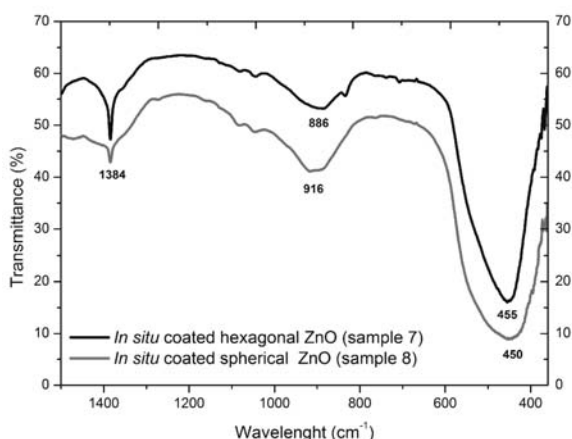


Figure 14b: FTIR spectra of samples prepared with the *in situ* method for spherical and hexagonal nanoparticles.

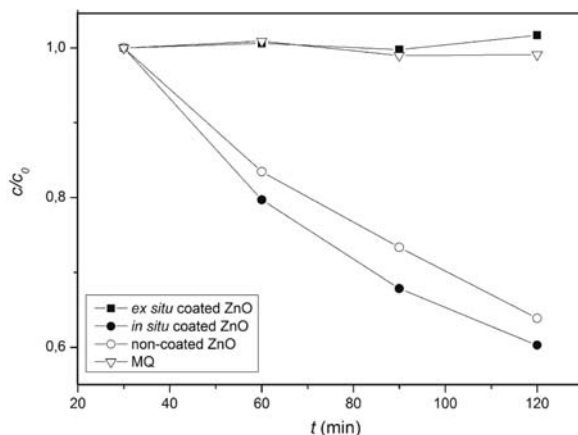


Figure 15: Photocatalytic degradation of caffeine as a function of time in the presence of non-coated ZnO or coated ZnO/silica particles.

ZnO nanoparticles exhibit some photocatalytic activity toward the oxidation of organic molecules. The photocatalytic degradation of caffeine, calculated as its relative concentration, is presented in Figure 15. According to Figure 15, ZnO/silica coated particles prepared with the *ex situ* method had negligible photocatalytic activity, which did not change over time. The photo stability of caffeine in the presence of the *ex situ* coated ZnO is similar to the caffeine photo stability in MQ water. Such behaviour was ascribed to the fact that the *ex situ* coated ZnO particles have the outer dense SiO₂ layers and are not catalytically active (Figure 15). In contrast, the non-coated or the *in situ* coated ZnO showed similar photocatalytic activity for the caffeine photo degradation. This fact suggests that with the *in situ* method practically no coverage of the ZnO was obtained that made such particles as active as non-coated ZnO. Similar observations were also reported for the degradation of caffeine with TiO₂.^{56,57}

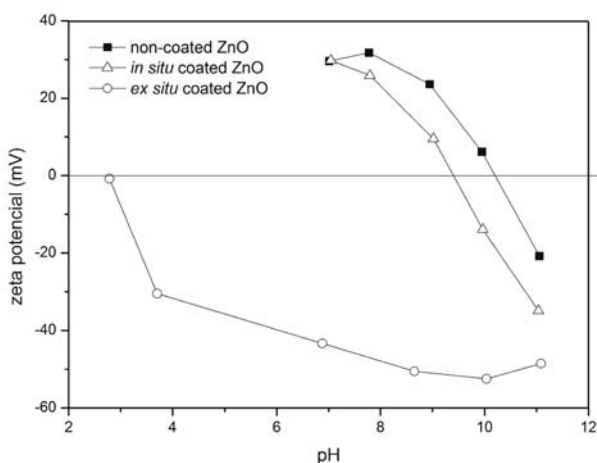


Figure 16: Zeta potential of ZnO, ZnO/silica (*in situ*) and ZnO/silica (*ex situ*).

Surface properties of coated and non-coated ZnO particles were measured with the zeta potential as a function of pH and are presented in Figure 16. The isoelectric point (IEP) of ZnO ranges from 8.7 to 10.3 and the zeta potential is positive below the (IEP) and negative above the (IEP).⁵⁸ The IEP of (SiO₂) ranges from 1.7 to 3.5.^{59,60} According to Figure 16, the *in situ* coated ZnO exhibited similar surface properties as non-coated ZnO, again implying a similar surface structure. These observed surface properties could be due to ZnO uncovered regions in the *in situ* sample.

The *ex situ* prepared coated ZnO samples, in contrast, exhibited completely different surface properties, very similar to pure silica surface, indicating excellent surface coverage of ZnO with silica. Prepared ZnO samples with the *ex situ* or the *in situ* covering methods were used for the preparation ZnO/PMMA nanocomposites.

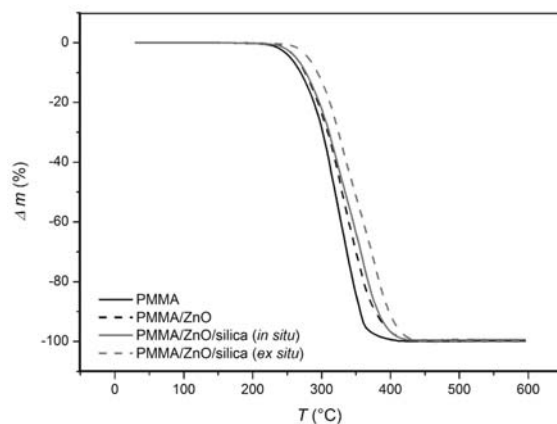


Figure 17: Thermal decomposition of PMMA and various ZnO/PMMA nanocomposites.

The thermal stability of the nanocomposites ZnO/PMMA prepared with non-coated or coated ZnO was studied using TG analysis. Activation energies of the ZnO/PMMA thermal decomposition were calculated using the non-linear isoconversional method. The isoconversional analysis is based on a kinetic model of the equation form:

$$\frac{\partial \alpha}{\partial t} = f(\alpha)k_{\alpha} \exp\left(-\frac{E_a}{RT}\right) \quad (1)$$

where $\frac{\partial \alpha}{\partial t}$ is conversion degree of the degradation reaction,

E_a is the apparent activation energy (J mol⁻¹), k_{α} is the pre-exponential factor (s⁻¹) and $f(\alpha)$ is the reaction model.⁶¹ From the above kinetic model, the linear dependence of $\ln \beta$ vs. $1/T$ may be recognized. Using the Doyle approximation,⁶¹ the slope in the $\ln \beta$ vs. $1/T$ diagram represents a value of $1.052 E_a / R$. Since thermal decomposition of the ZnO/PMMA composites may be described with only one process (Figure 17), diagrams of E_a as a function of α are presented in Figure 18.

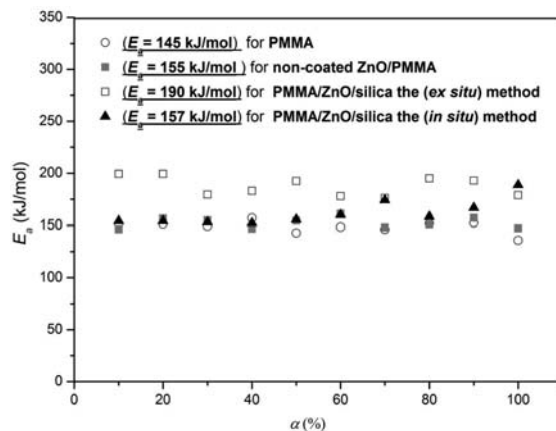


Figure 18: Calculated activation energies (E_a) of PMMA and various ZnO/PMMA nanocomposites.

By calculating the $E_a(\alpha)$ values of the investigated systems, it appeared that the addition of solid nanoparticles had two roles. On one hand, the addition of the *ex situ* coated ZnO nanoparticles represented a heat sink raising the temperature integral of the composite's thermal decomposition and consequently also raising its calculated E_a when compared to the pure PMMA ($E_a = 190$ kJ/mol for the *ex situ* ZnO/PMMA and $E_a = 145$ kJ/mol for pure PMMA). On the other hand, the introduction of the non-coated or the *in situ* coated ZnO nanoparticles into PMMA likewise represented a heat sink; however, ZnO also acts as a catalytically active surface, lowering the E_a of the PMMA thermal decomposition. Similar values of the calculated E_a for the non-coated ZnO/PMMA

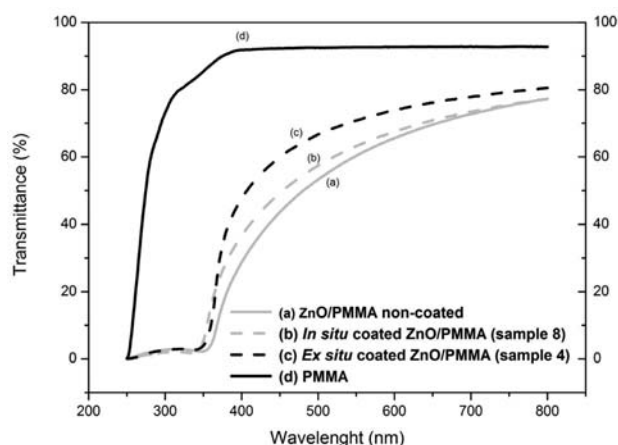


Figure 19: Light transmittance as a function of wavelength of (a) non-coated ZnO/PMMA, (b) and (c) coated ZnO/PMMA and (d) PMMA.

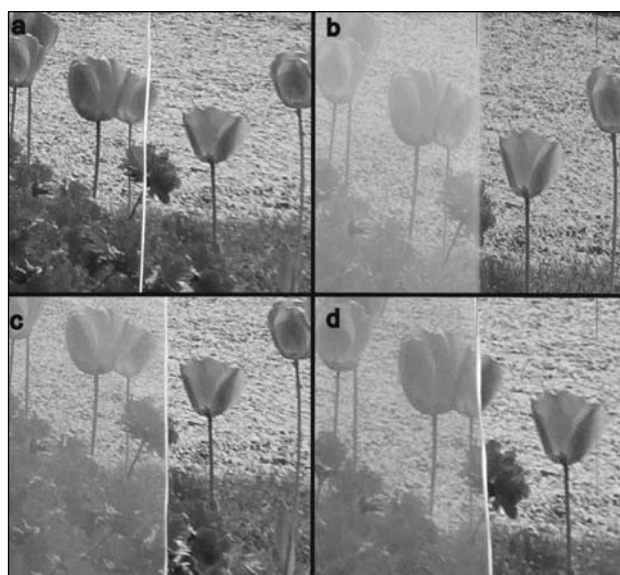
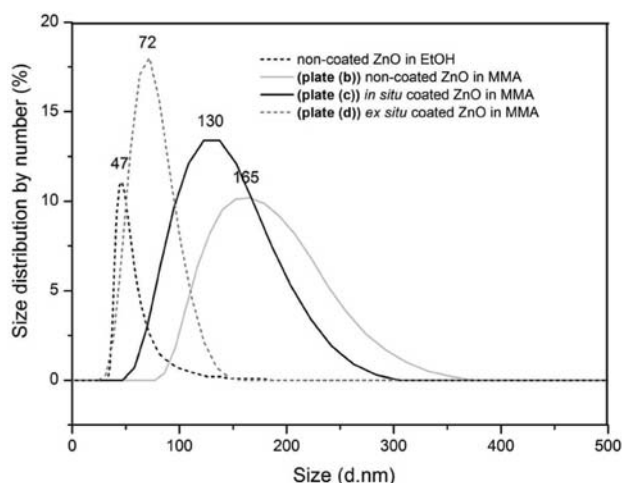


Figure 20: Left: Images of different plates prepared from a) PMMA, b) non-coated ZnO/PMMA, c) the *in situ* coated ZnO/silica/PMMA, and d) the *ex situ* coated ZnO/silica/PMMA. Right: DLS measurements of various ZnO nanoparticles measured in EtOH or MMA.

and the *in situ* coated ZnO/PMMA again imply the poor coverage of the ZnO with silica in the *in situ* process.

The ZnO/PMMA nanocomposites were also investigated with respect to their transparency for UV and visible light. Final composites should absorb UV light but transmit visible light. The transparency measurements were done on solid plates prepared from coated and non-coated ZnO particles into PMMA are presented in Figure 19. It appeared that any addition of ZnO nanoparticles into PMMA lowered the light transmittance through the composite. This reduction in light transmittance is less pronounced in the case of the *ex situ* coated ZnO introduction into PMMA and more pronounced in the cases of the *in situ* or non-coated ZnO introduction into PMMA. However, any addition of ZnO also substantially reduces light transmittance in the UV region.

The light transmittance reduction with solid particles introduction into PMMA is clearly demonstrated in (Figure 20). The highest transmittance among the ZnO/PMMA nanocomposites was measured in the case of the *ex situ* coated ZnO. Light transmittance of the prepared ZnO/PMMA plates can be correlated with the ZnO particle size distribution in the composites. It is evident that the non-coated or the *in-situ* coated ZnO particles tend to agglomerate when introduced into MMA. Consequently, thus prepared ZnO/PMMA plates exhibited lower transmittance. On the other hand, degree of agglomeration of the *ex situ* coated ZnO particles in MMA remains relatively low resulting in final ZnO/PMMA plate which is more transparent. The modus values of the ZnO in ethanol and the *ex situ* coated ZnO in MMA (as presented in the DLS curves) are 47 and 72 nm, respectively, implying that the *ex-situ* coated ZnO is well dispersed in PMMA.



4. Conclusions

The two different morphologies of ZnO nanoparticles (hexagonal and spherical) were prepared by varying the solvent ratio (water to ethylene glycol). The prepared ZnO nanoparticles were coated *ex situ* or *in situ* with silica. We observed that different concentrations of TEOS during the *ex situ* coating process affected the thickness of the silica layer around ZnO-core. In contrast, the *in situ* coating method influenced both the formed particles' morphology and their phase composition without yielding clear ZnO-core and SiO₂-shell structure. The effectiveness of SiO₂ coating was also followed with photocatalytic degradation of caffeine on the ZnO/SiO₂ particles. The *ex situ* coated ZnO particles were catalytically non-active while the *in situ* coated ZnO catalytically degraded caffeine similarly to the non-coated ZnO. Various catalytic activities are related to different surface properties of particles. The *ex situ* coated ZnO had similar surface properties as pure SiO₂ indicating dense SiO₂-shell on ZnO-core. In contrast, surface properties of the *in situ* coated ZnO were similar to the surface properties of the non-coated ZnO. Any addition of treated ZnO into PMMA lowered light transmittance of the composites compared to pure PMMA material. The highest light transmittance was measured in the case of the *ex situ* coated ZnO introduction into the composite due to relatively good solid particle dispersion. Such composite ZnO/PMMA materials have potential applications as UV protectors and thermally stabilized plexiglas.

5. Acknowledgements

The authors gratefully acknowledge the financial support of the Slovenian Research Agency (programme P1-0030). We acknowledge the financial support from the Ministry Education, Science, Culture and Sport of the Republic of Slovenia through the contract No. 3211-10-000057 (Centre of Excellence for Polymer Materials and Technologies).

6. References

1. N. Sounderya, Y. Zhang, *Recent. Pat. Biomed. Eng.* **2008**, *1*, 34–42.
2. H. M. Lin, S. J. Tzeng, P. J. Hsiau, W. L. Tsai, *Nanostruct. Mater.* **1998**, *10*, 465–477.
3. J. Q. Xu, Q. Y. Pan, Y. A. Shun, Z. Z. Tian, *Sensor. Actuat. B-Chem.* **2000**, *66*, 277–279.
4. M. Bitenc, M. Marinsek, Z. C. Orel, *J. Eur. Ceram. Soc.* **2008**, *28*, 2915–2921.
5. Y. L. Wu, A. I. Y. Tok, F. Y. C. Boey, X. T. Zeng, X. H. Zhang, *Appl. Surf. Sci.* **2007**, *253*, 5473–5479.
6. M. Bitenc, P. Podbrscek, Z. Crnjak Orel, M. A. Cleveland, J. A. Paramo, R. M. Peters, Y. M. Strzhemechny, *Cryst. Growth. Des.* **2009**, *9*, 997–1001.
7. S. Baruah, J. Dutta, *Sci. Technol. Adv. Mat.* **2009**, *10*, 013001–013019.
8. X. Xu, H. Pang, Z. Zhou, X. Fan, S. Hu, Y. Wang, *Adv. Powder Technol.* **2011**, *22*, 634–638.
9. Y. Kim, S. Kang, *Acta Mater.* **2011**, *59*, 3024–3031.
10. T. Shishido, Y. Yamamoto, H. Morioka, K. Takaki, K. Takehira, *Appl. Catal. A* **2004**, *263*, 249–253.
11. X. Y. Zhao, B. C. Zheng, C. Z. Li, H. C. Gu, *Powder Technol.* **1998**, *100*, 20–23. ŠRTF bookmark end: č_ENREF_11
12. H. L. Shen, X. B. Lou, Z. Hui, B. B. Li, *T Nonferr. Metal. Soc.* **2007**, *17*, S814–S817.
13. M. J. Alam, D. C. Cameron, *J. Sol-Gel Sci. Technol.* **2002**, *25*, 137–145.
14. T. Wen, J. P. Gao, J. Y. Shen, Z. S. Zhou, *J. Mater. Sci. Technol.* **2001**, *36*, 5923–5926.
15. L. Gao, Z. T. Chen, *J. Cryst. Growth* **2006**, *293*, 522–527.
16. K. H. Tam, C. K. Cheung, Y. H. Leung, A. B. Djuricic, C. C. Ling, C. D. Beling, S. Fung, W. M. Kwok, W. K. Chan, D. L. Phillips, L. Ding, W. K. Ge, *J. Phys. Chem. B* **2006**, *110*, 20865–20871.
17. B. Wen, Y. Huang, J. J. Boland, *J. Phys. Chem C* **2008**, *112*, 106–111.
18. M. Bitenc, Z. C. Orel, *Mater. Res. Bull.* **2009**, *44*, 381–387.
19. D. Japic, J. A. Paramo, M. Marinsek, Y. M. Strzhemechny, Z. C. Orel, *J. Lumin.* **2012**, *132*, 1589–1596.
20. J. Zhai, X. Tao, Y. A. Pu, X. F. Zeng, J. F. Chen, *Appl. Surf. Sci.* **2010**, *257*, 393–397.
21. M. Nakade, M. Ogawa, *J. Mater. Sci. Technol.* **2007**, *42*, 4254–4259.
22. J. Wang, T. Tsuzuki, B. Tang, P. Cizek, L. Sun, X. Wang, *Colloid Polym. Sci.* **2010**, *288*, 1705–1711.
23. L. Spanhel, *J. Sol-Gel Sci. Technol.* **2006**, *39*, 7–24.
24. M. Bitenc, G. Dražić, Z. Crnjak Orel, *Cryst. Growth Des.* **2010**, *10*, 830–837.
25. K. Han, Z. Zhao, Z. Xiang, C. Wang, J. Zhang, B. Yang, *Mater. Lett.* **2007**, *61*, 363–368.
26. T. Ung, L. M. Liz-Marzan, P. Mulvaney, *Langmuir* **1998**, *14*, 3740–3748.Š
27. L. SelegArd, V. Khranovskyy, F. Soderlind, C. Vahlberg, M. Ahren, P. O. Kall, R. Yakimova, K. Uvdal, *ACS Appl. Mater. Interfaces* **2010**, *2*, 2128–2135.
28. S.-r. Ma, L.-y. Shi, X. Feng, W.-j. Yu, B. Lu, *J. Shanghai Jiaotong Univ.* **2008**, *12*, 278–282.
29. E. J. Tang, S. Y. Dong, *Colloid Polym. Sci.* **2009**, *287*, 1025–1032.
30. C. M. Halliwell, A. E. G. Cass, *Anal. Chem.* **2001**, *73*, 2476–2483.
31. S. Liu, L. Luc, Z. Yang, P. Cool, E. F. Vansant, *Mater. Chem. Phys.* **2006**, *97*, 203–206.
32. I. A. M. Ibrahim, A. Zikry, M. A. Sharaf, *J. American Sci.* **2010**, *6*, 985–989.
33. K. D. Kim, H. T. Kim, *J. Sol-Gel Sci. Technol.* **2002**, *25*, 183–189.

34. A. Lenz, L. Selegard, F. Soderlind, A. Larsson, P. O. Holtz, K. Uvdal, L. Ojamae, P. O. Kall, *J. Phys. Chem. C* **2009**, *113*, 17332–17341.
35. G. Kickelbick, *Prog. Polym. Sci.* **2003**, *28*, 83–114.
36. B. Kulyk, V. Kapustianyk, V. Tsybulskyy, O. Krupka, B. Sahraoui, *J. Alloys Compd.* **2010**, *502*, 24–27.
37. Z. H. Guo, S. Y. Wei, B. Shedd, R. Scaffaro, T. Pereira, H. T. Hahn, *J. Mater. Chem.* **2007**, *17*, 806–813.
38. C. H. Hung, W. T. Whang, *J. Mater. Chem.* **2005**, *15*, 267–274.
39. T. Tanaka, *Ieee T Dielect. El. In* **2005**, *12*, 914–928.
40. L. Q. Zhang, Y. Z. Wang, Y. Q. Wang, Y. Sui, D. S. Yu, *J. Appl. Polym. Sci.* **2000**, *78*, 1873–1878.
41. T. Wang, W. Hwang, M. Yeh, *J. Appl. Polym. Sci.* **2006**, *104*, 4135–4143.
42. R. C. Patil, S. Radhakrishnan, *Prog. Org. Coat.* **2006**, *57*, 332–336.
43. A. Anžlovar, Z. C. Orel, M. Žigon, *Eur. Polym. J.* **2010**, *46*, 1216–1224.
44. P. Maiti, P. H. Nam, M. Okamoto, N. Hasegawa, A. Usuki, *Macromolecules* **2002**, *35*, 2042–2049.
45. M. M. Demir, M. Memesa, P. Castignolles, G. Wegner, *Macromol. Rapid Commun.* **2006**, *27*, 763–770.
46. J. A. Paramo, Y. M. Strzhemechny, A. Anžlovar, M. Žigon, Z. Crnjak Orel, *J. Appl. Phys.* **2010**, *108*, 023517–023523.
47. X. W. Du, Y. S. Fu, J. Sun, X. Han, J. Liu, *Semicond Sci. Technol.* **2006**, *21*, 1202–1206.
48. V. Khrenov, F. Schwager, M. Klapper, M. Koch, K. Müllen, *Polym. Bull.* **2007**, *58*, 799–807.
49. E. J. Tang, G. X. Cheng, X. L. Ma, *Adv. Powder Technol.* **2006**, *161*, 209–214.
50. R. Y. Hong, J. Z. Qian, J. X. Cao, *Powder Technol.* **2006**, *163*, 160–168.
51. S. Li, M. S. Toprak, Y. S. Jo, J. Dobson, D. K. Kim, M. Muhammed, *Adv. Mater.* **2007**, *19*, 4347–4352.
52. F. Rubio, J. Rubio, J. L. Oteo, *Spectrosc. Lett.* **2011**, *31*, 199–219.
53. P. Podbršček, G. Dražić, A. Anžlovar, Z. Crnjak Orel, *Mater. Res. Bull.* **2011**, *46*, 2105–2111.
54. J. C. Hurt, C. J. Phillips, *J. Am. Ceram. Soc.* **1970**, *53*, 269–273.
55. L. Chung-Cherng, S. Pouyan, *J. Non-Cryst. Solids* **1994**, *171*, 281–289.
56. I. Dalmázio, L. S. Santos, R. P. Lopes, M. N. Eberlin, R. Augusti, *Environ. Sci. Technol.* **2005**, *39*, 5982–5988.
57. L. C. Chuang, C. H. Luo, S. W. Huang, Y. C. Wu, Y. C. Huang, *Adv Mater Res* **2011**, *214*, 97–102.
58. G. A. Parks, *Chem Rev* **1965**, *65*, 177–197.
59. P. Wilhelm, D. Stephan, *J. Photochem. Photobiol. A: Chem* **2007**, *185*, 19–25.
60. M. Kosmulski, Book Chemical properties of material surfaces, Marcel Dekker, New York, **2001**.
61. A. Laachachi, M. Ferriol, M. Cochez, D. Ruch, J. M. Lopez-Cuesta, *Polym. Degrad. Stab.* **2008**, *93*, 1131–1137.

Povzetek

Nanodelci ZnO so bili pripravljani po enostopenjskem sinteznem postopku, kjer smo spreminjali volumensko razmerje topil voda/etilen glikol. Morfološka analiza (SEM in TEM) je pokazala, da so v pripravljenih produktih prisotni nanodelci ZnO heksagonalne in sferične oblike. Pripravljene nanodelce ZnO smo oplaševali *in-situ* ali *ex-situ* z reagentom tetraetil-ortosilikat (TEOS). Debelina plašča SiO₂ okoli nanodelcev ZnO se je gibala med 4 in 18 nm. Oplaščene in neoplaščene nanodelce ZnO smo v nadaljevanju okarakterizirali z različnimi analiznimi metodami. Nanodelce ZnO smo uporabili tudi za pripravo nanokompozita PMMA/ZnO. Izkaže se, da so nanokompoziti PMMA/ZnO relativno dobro prepustni za vidno svetlobo, hkrati pa relativno dobro absorbirajo UV svetlobo v območju 250–370 nm.